Article

Cyanobacterial Pigments as Natural Photosensitizers for Dye-Sensitized Solar Cells

Tatiana Montagni [1], Mauricio Ávila [1], Sofía Fernández [2], Sylvia Bonilla [2] and María Fernanda Cerdá [1,*]

1   Laboratorio de Biomateriales, Instituto de Química Biológica, Facultad de Ciencias, UdelaR. Iguá 4225, Montevideo 11400, Uruguay; tmontagni@fcien.edu.uy (T.M.); mavila@fcien.edu.uy (M.Á.)
2   Sección Limnología, Instituto de Ecología y Ciencias Ambientales, Facultad de Ciencias, UdelaR. Iguá 4225, Montevideo 11400, Uruguay; sbon@fcien.edu.uy (S.B.)
*   Correspondence: fcerda@fcien.edu.uy

Abstract: Three filamentous freshwater cyanobacterial strains were grown at high light intensity to produce lipidic dyes composed of xanthophylls, carotenes, and chlorophyll a. The properties of the pigments were evaluated as suitable natural compounds to be applied in dye-sensitized solar cells (DSSC). The assembled DSSC were characterized using the density current vs. potential profiles and electrochemical impedance spectroscopy. With an efficiency of 0.127%, our results are higher than those previously reported using similarly structured compounds from natural sources such as algae and cyanobacteria, among others. The best efficiencies were probably related to myxoxanthophyll-like derivates and aphanizophyll are carotenoids with many hydroxyl groups being able to interact with the semiconductor surface. The stability of the bonding between the dyes and the titanium oxide of the photoelectrode is crucial to ensuring the acceptable performance of the DSSC, which was successfully achieved in our experiments with carotenoids with many hydroxyl groups. Our results point to cyanobacterial pigments as a promising source of natural dyes for use in solar cells.

Keywords: glycosidic carotenoids; electrochemical; impedance; spectroscopy; natural dyes

1. Introduction

Since being first reported in the 1990s, dye-sensitized solar cells (DSSC) have been the focus of thousands of reports [1–8]. In a world of growing environment-friendly options, photovoltaic (PV) applications are still very limited, accounting for around 5% of the electricity production from alternative energy sources, behind hydropower and wind [9,10]. However, the costs associated with the manufacture and application of solar PV cells are decreasing, which is expected to increase the installation of such devices significantly in the coming years [11,12].

When it first appeared, the costs associated with DSSC production were lower than those of silicon. Nowadays, as costs related to the fabrication and installation of traditional solar silicon panels are decreasing, the application of DSSC technology is linked to the DSSC's particular structural characteristics. Because DSSC are translucent, they can be used as power-generating building blocks [13–18]. They can be applied in BIPV buildings without special space requirements, as curtains or indoors, as well as in "greenhouse" structures. Nevertheless, DSSC allow for a unique opportunity: the exploitation of natural dyes from accumulated organic waste such as seaweeds, discarded fruits, or leaves associated with tree exploitation [19,20]. Natural dyes can be extracted using simple and low-cost methods [21–24]. Many natural dyes have been explored as sensitizers with wide chemical structural diversity, like anthocyanins, xanthophylls, carotenes, and phycobiliproteins, among others [25–30].

The DSSC comprises two flat electrodes with a liquid electrolyte containing a redox couple between them in a sandwich configuration [31–33]. The photoanode is one of the main pieces and contains a nano-structured semiconductor (usually TiO_2) with a sensitizer

(a pigment or a mixture of them) adsorbed to the surface. The assembly semiconductor/pigment plays a crucial role in the performance of the photovoltaic cell, and this electrode surface must be fully covered to ensure the best electron transfer. When sunlight hits the dye, electrons are released and transferred to the semiconductor and then to the conductive glass (usually FTO, fluorine-doped tin oxide), where the TiO_2 is deposited, generating the photocurrent. However, undesired paths are always present in a DSSC, lowering the cell's efficiency [34,35]. Electrons promoted to higher energy levels of the dye can return to the original ground state, resulting, for example, in fluorescence decay, among other effects. Furthermore, once in the TiO_2, the electrons could be transferred back to the dye or directly to the redox couple of the electrolyte. These two processes, known as recombination, are the main reason for the decline in the measured efficiencies for the DSSC. Understanding and addressing these issues is therefore critical to the advancement of DSSC technology.

Natural dyes have many relevant properties that allow them to be used as sensitizers, but they also suffer from more disadvantages than synthetic dyes. Reported power conversion efficiencies (PCE) are therefore low, particularly when compounds such as xanthophylls or carotenes are used as sensitizers [36–40]. However, and as explained above, the low-cost methods associated with their extraction and the fact that they offer an alternative means of profiting from accumulated organic waste are the points that are most interesting in exploring natural dyes as sensitizers.

Cyanobacteria are a large group of photolithotrophic bacteria with remarkably high pigment diversity, including hydrosoluble phycobiliproteins and lipophilic carotenoids involved in different cellular/biological functions [41,42]. Many of these pigments are also found in algae, while others are exclusively prokaryotic. Cyanobacteria are present in almost all illuminated habitats and are particularly successful in freshwater phytoplankton [43], making them a potentially attractive source of natural dyes with technological applications for solar cells [36].

In this work, three filamentous freshwater cyanobacterial strains were grown under high light intensity to produce different mixtures of lipidic dyes, mainly composed of xanthophylls, carotenes, and chlorophyll a. With an efficiency of 0.127%, our results are higher than those previously reported using similarly structured compounds from natural sources such as algae and cyanobacteria, among others.

2. Materials and Methods

2.1. Extraction of Lipidic Pigments

Three filamentous cyanobacterial strains isolated from different regions were selected for the study: MVCC19 (*Raphidiopsis raciborskii*, Nostocales, planktonic, from Uruguay); D3267 (*Dolichospermum* sp., Nostocales, planktonic, from Brazil); and PCCC_E5 (E5) (*Phormidium* sp., Oscillatoriales, benthic, from Canada) [44,45]. These strains are rich in glycosidic carotenoids and ketocarotenoids (hydro-echinenone (3'-hydroxyechinenone) and myxoxanthophyll (myxol 20-glycosides)) [46], in MVCC19 and D3267 [44], and in unknown myxoxanthophyll-like and oscillaxanthin-like derivatives in E5 [47]. All three strains also have unknown myxoxanthophyll-like carotenoids (myxol glycoside type 1) (not characterized) and a high contribution of β,β-carotene [44]. Static cultures were kept in a modified BG11 medium [48] at 24 °C, under PAR light intensity from 10 to 30 μmol photons $m^{-2}s^{-1}$, and with a 12:12 photoperiod. To obtain the lipid extracts (dyes), 20 mL of the strains were spread on culture flasks (in duplicates) and placed in an incubator chamber set at 24 °C with continuous PAR light. They were acclimated in subsequent light intensity increments to reach a final 300 μmolphotons $m^{-2}s^{-1}$ in the following pattern: 3, 4, 4, and 12 days at 40, 65, 180, and 300 μmolphotons $m^{-2}s^{-1}$, respectively. Cultures were shaken and resettled every 48 to 72 h during the entire period, and their condition was visually inspected, corroborating their growth as described in [44].

Under dim light conditions, 5 mL of each culture was filtered through GFC glass fiber filters and immediately frozen at −20 °C. Lipidic pigments were extracted in hot 90%

ethanol according to the ISO 1992 method. The extracts were then clarified via filtration (syringe with GFC glass fiber filters) and kept at -20 °C until further analysis. Purified β,β-carotene acetone solutions (extracted from spinach leaves, [49]) were also used to compare the behavior of sensitizers with and without suitable functional groups to establish bonds with the titania.

The influence of the dye concentration in the sensitization step on the power conversion efficiency of the assembled cells was evaluated. For this, extracts of D3267, MVCC19, and β,β-carotene with different concentrations in the lipidic pigments, obtained from the evaporation of the solvent at 40 °C (in an open electric oven), were used. According to our previous results, thermogravimetric and differential scanning calorimetric techniques proved the stability of the ether bonds and terpenes structures as fucoxanthin until reaching the temperature of 100 °C [20,50]. Moreover, the solutions' absorbance spectra and cyclic voltammetric profiles were measured and compared before and after evaporation until reaching the desired absorbance maxima values.

2.2. Characterization

The visible spectra were obtained by scanning the solutions from 350 to 750 nm (by 0.05 nm) using an Analytic-Jena SPECORD 200 Plus spectrophotometer. Fluorescence spectra were also acquired using a FluoroMax4 (HORIBA, Jobin Yvon, Minami-ku Kyoto, Japan) spectrofluorometer. Excitation–emission matrices (EEMs) were obtained within the range of 200–750 nm for excitation and 250–800 nm for emission.

Cyclic voltammetric measurements were performed, employing a CHI 604E potentiostat and using screen-printed disposable Au-*pc* (polycrystalline) electrodes (DROPSENS) at potential scan rates (v) between 0.02 and 0.05 Vs^{-1}, with a pseudo-reference potential of E = 0.24 V vs. SHE (standard hydrogen electrode). The supporting electrolyte was ethanol/0.1 M NaClO$_4$ in milli-Q water (50/50).

2.3. DSSC Assembly and Characterization

Photoanodes were prepared through the immersion of the FTO/TiO$_2$ (SOLARONIX test kit, 20 mm × 20 mm sized, active area of mesoporous TiO$_2$ 0.36 cm^2, Solaronix, Aubonne, Switzerland) electrodes overnight in dyes' containing the solution; then, the samples were rinsed thoroughly with ethanol. As explained above, the lipidic pigments extracted from the cyanobacterial strains MVCC19, D3267, and E5 contained ethanol, whereas the β,β-carotene was an acetone solution. For comparison purposes, DSSC sensitized with the N3 dye (Greatcell Solar, Queanbeyan, Australia) as a sensitizer were constructed and characterized under identical conditions to the pigments mentioned in our present work. Before use, the FTO/TiO$_2$ electrode was heated at 500 °C for 30 min. The titania opaque electrode comprises two films printed on TCO22-7/LI glass (7 Ω/sq fluorine-doped tin oxide coating on one side). The first one is the active layer, is about 10 microns thick, and contains anatase nanoparticles of about 15–20 nm (porosity ~10–20 nm). The second film is reflective, with a thickness of about 2–3 microns and composed of about 80–120 nm nanoparticles.

A sandwich configuration was used, with the FTO/TiO$_2$ photonode placed parallel to the FTO/Pt counter (20 mm × 20 mm sized, screen printed with SOLARONIX's Pt Platinum Catalyst). The cell was then completed by the addition of a liquid electrolyte (50 mM iodide/tri-iodide in acetonitrile, SOLARONIX Iodolyte AN-50).

To characterize the DSSC, the current density vs. voltage (J-V) profiles were measured using a CHI 604E potentiostat at a potential scan rate (v) of 0.05 Vs^{-1} at room temperature in the dark using a solar simulator from ABET Technologies (100 mW cm^{-2}, 1.5 AM). Complementary data were assessed from the electrochemical impedance spectroscopy (EIS) results, performed between 0 and 0.5 V and within the frequency range of 0.1 Hz to 3 MHz (in the dark).

3. Results

Understanding the primary composition of the compounds is important as it determines the presence or absence of suitable functional groups for establishing bonds with titanium in their chemical structure. The presence of at least two -OH groups attached to carbon rings is a promising indication for the formation of stable and robust coordination bonds to the titanium of the semiconductor nanostructured net. The characterization techniques applied to the lipidic pigments in this section offered accurate ways of detecting their chemical composition [51].

3.1. Visible Absorbance Spectroscopy

The recorded spectra for the different pigment extracts were superimposed for comparison purposes, fixing the absorbance values at 475 nm in 1 (Figure 1). For this, some solutions were evaporated at 40 °C, whereas others were graphically normalized (Figure 1).
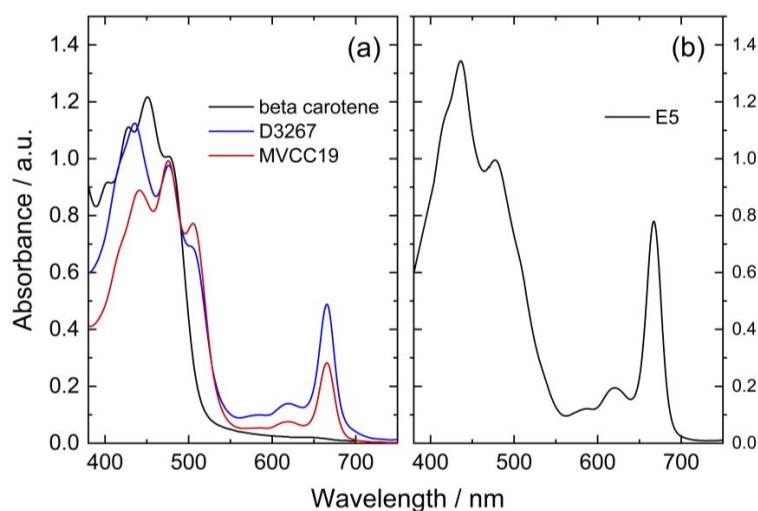
Figure 1. (**a**) Visible absorbance spectra of lipidic pigment extracts from two cyanobacterial strains in ethanol (blue: D3267; red: MVCC19) and β,β-carotene in acetone (black line) recorded after evaporation at 40 °C. (**b**) Normalized spectra (to absorbance at 475 nm) of the lipidic extract obtained from the E5 strain in ethanol.

In order to discuss the composition of the extracts analyzed, it is necessary to have a look at the structure of the main pigments (Table 1) that have been detected in these strains in previous studies [44].

It is natural to expect high concentrations of chlorophyll a in the extracts used as they are derived from cyanobacteria [43]. Chlorophyll a is highly labile at high temperatures and is expected to have degraded significantly during the evaporation process. The ratio between the initial amount of carotenoids and chlorophyll a consequently changed after evaporation.
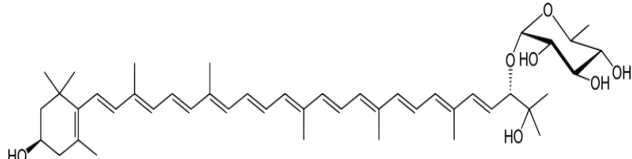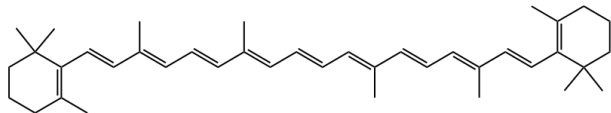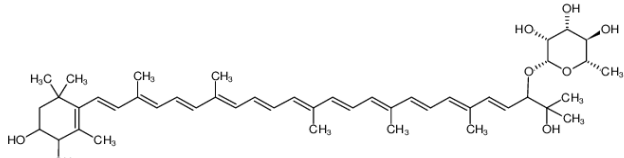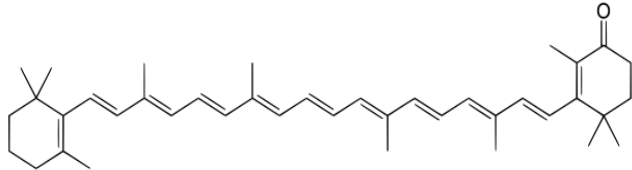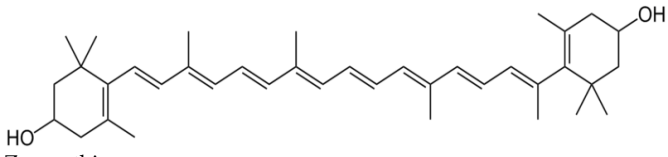
The peaks at 475 nm can be explained by the presence of different xanthophylls in the extracts, such as myxoxanthophyll-like derivates and aphanizophyll, making these extracts highly valuable as sensitizers due to the presence of -OH moieties that can bind the titanium (Table 1).

The three strains had distinctive absorption spectra with different peaks indicating specific pigments signatures. Among the analyzed samples, pigments extracted from strain E5 had the highest absorbance values at 617 and 666 nm (Figure 1). It is reported that chlorophyll a (CHL) displays absorbance maximum peaks at 400, 585, 617, and 666 nm [52]. Consequently, it was inferred that the extracts of this strain contained more CHL than the other ones. Additionally, the E5 extract presented a peak at 435 nm with higher absorbance than the peak observed in the other strains and a shoulder at 410 nm. The spectra of E5 could then be explained by a high content of beta carotene, echinenone, and zeaxanthin, as previously reported for this strain (Table 1) [53–55].

For the MVCC19 extract, the absorbance peak at 507 nm was higher than the one observed for the D3267 extract (not detected in E5). Significant contents of myxoxanthophyll-like derivates and aphanizophyll could be a suitable explanation according to the absorption spectra signature of these carotenoids and the reported bibliographic data (Table 1) [56,57]. Moreover, the extract from MVCC19 showed the lowest content in CHL, and a shoulder at 410 nm was also detected. Previous results support our hypothesis, where the glycoside carotenoids, as myxol derivatives, and aphanizophyll were abundant, and beta carotene and the ketocarotenoid echinenone were also present [44]. Myxoxanthophyll is almost exclusively found in cyanobacteria, and its name includes a group of different/varieties of xanthophyll glycosides characterized by rhammose as the dominant sugar moiety and a hexose with a high number of conjugated double bonds [58,59], which makes it a suitable molecule for DSSC. As myxoxanthophylls are very abundant in some cyanobacteria and are involved in the photoprotection and stabilization of the cell envelope [60], these molecules have great potential for further studies in the search for new natural dyes for solar cells.

The absorption spectrum of D3267 pigments was intermediate between those of the other strains. This strain was characterized by high absorbance values at 435 nm, low absorbance values at 507 nm, and the absence of a shoulder at 410 nm. The D3267 extract was potentially composed of myxol derivatives, and the observed spectra arose mainly from the presence of this compound.

Table 1. Main structure of the pigments inferred to be present in the analyzed extracts, with their absorption peaks as reported in the literature (measured in methanol) [42,53–55].

Structure	Maximum Absorption/nm
Myxoxanthophyll	450, 474, 506
β,β-carotene	(400) shoulder, 425, 450, 477
Aphanizophyll	450, 477, 508
Echinenone	460 (broad)
Zeaxanthin	426, 453, 480

3.2. Electrochemical Evaluation of the Extracts

Cyclic voltammetric profiles of the samples were performed at 0.02 and 0.05 Vs^{-1}. As the extracts were composed of different mixtures of pigments, electrochemical profiles were also composed of signals arising from the superimposed contributions of all the electroactive moieties. The electroactive groups of the evaluated molecules are presumably ketone groups (-C=O), hydroxyl (-OH), conjugated double bounds (-C=C-), and ethers (-O-). Differences between the first recorded potential scan and subsequent ones were observed in the anodic region. For instance, the broad peaks observed in the first scan were found to be divided into two distinct contributions in the stable register reached after at least three scans within the same potential range. The reduction in the original compounds was successfully achieved in the cathodic region (Figure 2).
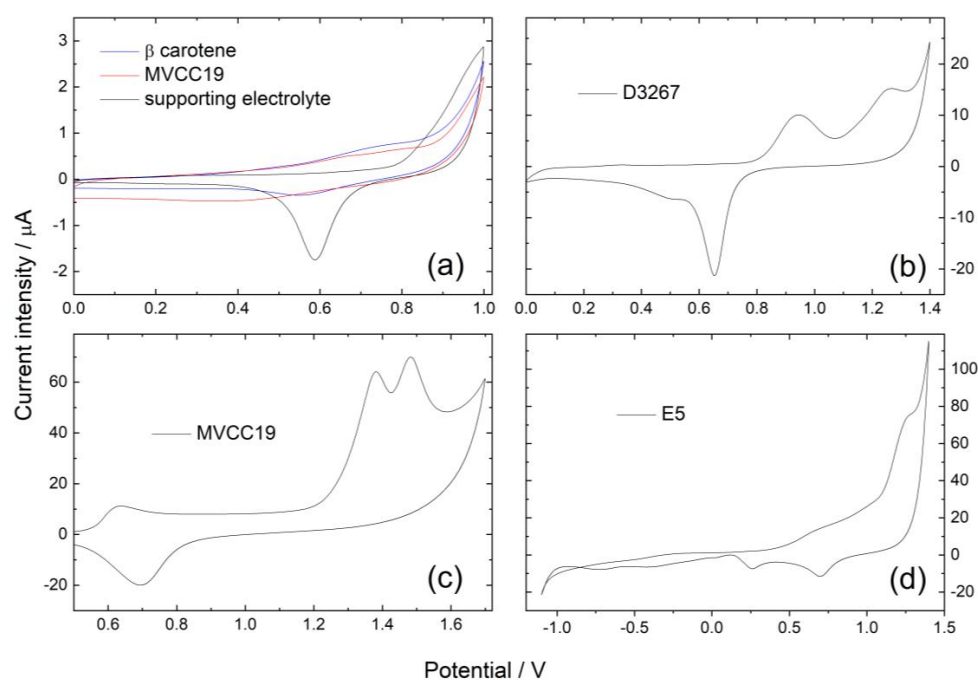
Figure 2. Cyclic voltammetric profiles for Au-*pc* in (**a**) beta carotene and MVCC19; (**b**) D326; (**c**) MVCC19; and (**d**) E5 in the supporting electrolyte (ethanol/0.1 M NaClO$_4$ in milli-Q water 50/50. v = 0.02 Vs^{-1}. Pseudo-reference potential of E = 0.24 V vs. SHE (standard hydrogen electrode).

Voltammetric profiles for Au-*pc* in beta carotene displayed only one anodic contribution at 0.75, with the cathodic one at −1.05 V (Figure 2, Table 2). As previously reported, the oxidation of β,β-carotene proceeds in one apparent irreversible oxidation step involving an exchange of two electrons per molecule [61–63]. The formation of a radical cation is followed by the formation of an epoxide. The electrochemical reaction proceeds in one apparent oxidation step involving carbons at positions 15 and 16 in the chain; both reactions proceed at almost the same time, and the two electrons are transferred in one step.

The voltammetric profiles for the MVCC19 extract showed three prominent anodic current intensity peaks: a broad peak at 0.70 V (that could split in two contributions, at 0.72 and 0.84 V in the following scans); a peak ranging between 0.90 and 1.10 V (depending on the potential scan rate v); and a third broad one at 1.25 V (divided in two contributions at 1.36 and 1.42 V) (see Figure 2). The main cathodic intensity current peak was detected at −0.78 V. Contributions at 0.72 and 0.84 V could arise from the presence of beta carotene and echinenone (with a reported redox behavior similar to the first one) [61]. The peak in the range of 0.90 to 1.10 could be explained by the chlorophyll redox behavior [64,65]. The contributions at 1.36 and 1.42 V are the most relevant because of their high intensity. They are explained by the oxidation of the -OH groups from the myxoxanthophyll-like derivates and aphanizophyll, occurring at slightly different potentials (those coming from

the glycoside differ from those attached to the main long-chain) and even superimposed on the ether oxidation [61,63,65–68].

Table 2. Summary of the main redox peaks detected at the analyzed dyes (MVCC19, D3267, E5, and β,β-carotene). The values between the brackets belong to the stable profiles.

Dye	Anodic/V	Assignation	Cathodic/V
MVCC19	0.70 (0.72 and 0.84) 0.90–1.10 1.25 (1.36 and 1.42)	-C=C-(β,β-carotene) CHL -OH and -O-	−0.78
D3267	0.95 1.3	CHL -OH	−1.0
E5	0.70 0.95 1.27 (1.30 and 1.40)	-C=C-(β,β-carotene) CHL -OH and -O-	−0.75
β,β-carotene	0.75	-C=C-	−1.05

For the D3267 extract, two anodic contributions were observed at 0.95 V and 1.30 V, with the cathodic peak at −1.00 V (Figure 2). The first anodic peak was assessed for the presence of chlorophyll, whereas the peak at 1.30 was assigned to the oxidation of the -OH groups from the myxoxanthophyll-like derivates.

In the case of the dyes of E5, the anodic peaks were found at 0.70 V, 0.95 V, and 1.27 V (split into 1.30 and 1.40 V in the following scans), and the cathodic contribution was detected at −0.75 V (Figure 2).

In summary, the presence of β,β-carotene (or echinenone, because of their almost identical redox behavior) is clearly detected using the cyclic voltammetry technique in the case of MVCC19 and E5 but not in the case of D3267 (Table 2). The three analyzed strains also verified chlorophyll, as expected. The employed technique also detected the presence of -OH moieties, particularly in MVCC19, where the intensity current peaks arising from their redox behavior were clearly defined. The detection of -OH groups and the values of the measured oxidation and reduction potentials (as will be further discussed) again highlight the potential of the here-analyzed extracts for this type of biotechnological application.

3.3. Electrochemical Evaluation of the DSSC

To compare the different assembled cells (no matter which dye is applied), the absorbance of the peak at 475 nm was chosen as a marker. The analysis of the DSSC's measured efficiencies performed in this text centers on those cells with an absorbance at 475 nm within the 0.8-to-1.0 range. DSSC sensitized via dye solutions with absorbance values lower than 0.6 showed lower power conversion efficiency (PCE) values. Figure 3 displays current densities (J) vs. potential profiles for the most efficient cells containing each sensitizer analyzed, whereas Table 3 shows the measured PCE and the main characteristics for the same cells. It is also necessary to combine the data from the visible spectra and the cyclic voltammetry with the PCE of the measured cells to relate the efficiencies of the DSSC with the composition of the sensitizers.

The dyes should possess certain characteristics to ensure good PCE for the assembled cells. First, coordination through bond formation between the dye and the semiconductor must be achieved to allow for electron transference between the dye and the TiO_2. This bond has to be stable, and no desorption of the dye can be detected. Oxidation occurs after the light hits the pigment, and electrons are released. The LUMO values of the dye must, therefore, be higher than the conduction band-edge energy level of the TiO_2 electrode to ensure that the electron injection process is energetically favorable. The oxidation potentials of the dyes also need to be high enough (near 1 V) to ensure more-effective dye regeneration. Dye regeneration involves the $I_2^{-\bullet}/I^-$ redox couple (with a 0.9 V redox potential) and/or the I^-/I_3^- couple (0.35 V vs. SHE) [69]. Finally, the dyes must have very low fluorescence

emission to ensure that all the electrons produced are injected and then transported through the semiconductor network [19,21,70].
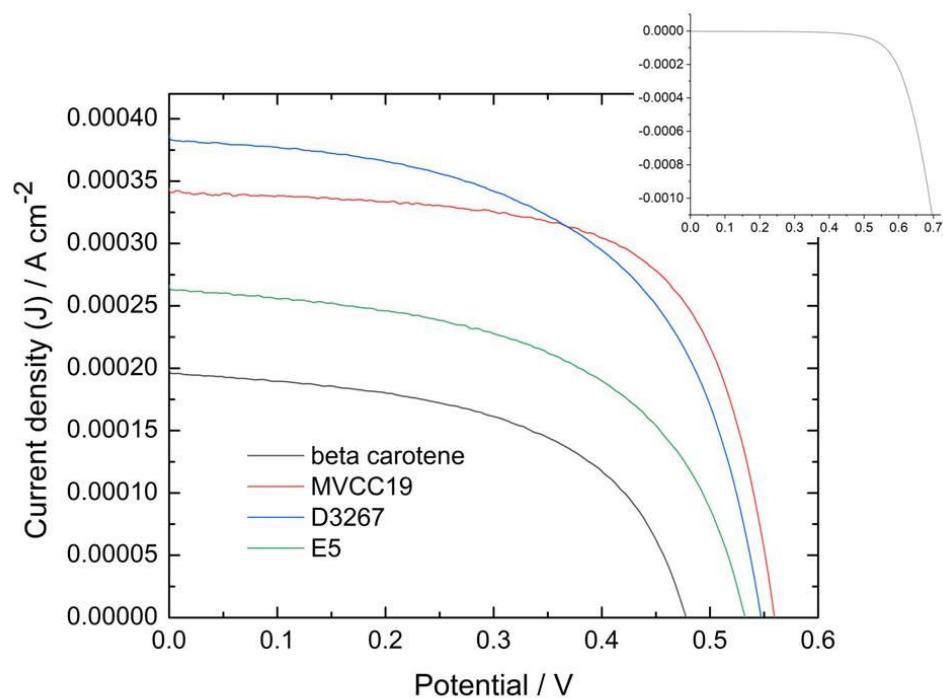
Figure 3. Photocurrent density vs. potential profiles for DSSC measured under one sun, AM 1.5 and $v = 0.05$ Vs^{-1} for the more-efficient cells sensitized with the different dyes mentioned in this work). Inset: dark current profile for the DSSC sensitized with MVCC19.

Table 3. Photovoltaic properties of cells assembled with different sensitizers. All measurements were performed under a sunlight intensity of 100 mW cm^{-2}, AM 1.5 G, and the active areas were 0.36 cm^2 for all the cells. Jsc is the short-circuit current density; Voc is the open circuit potential; FF is the fill factor; and η is the power conversion efficiency (PCE). The average values come from at least three independent assembled cells.

Property/Units	MVCC19	D3267	E5	β,β-Carotene
Jsc/Acm^{-2}	3.4×10^{-4}	3.8×10^{-4}	2.6×10^{-4}	1.9×10^{-4}
Voc/V	0.56	0.54	0.50	0.48
FF	0.67	0.57	0.53	0.51
η/%	0.127	0.120	0.078	0.048

In our study, cells sensitized with β,β-carotene were less efficient than those sensitized with the natural complex dyes because this compound does not have suitable groups with which to bind and coordinate to TiO$_2$ (as -OH, for example), and it has a long-chain structure [61]. When β,β-carotene was used, the photoanode surface was not fully covered, and some naked TiO$_2$ spots remained, affecting the electron transference and therefore the PCE of the measured cell [61–71]. Additionally, the β,β-carotene molecules were desorbed, as explained later in the EIS results. The oxidation redox potential of this compound was 0.75 V, coinciding with the reported one, but it was lower than the optimum (near 1 V) to ensure the dye regeneration.

The E5 dyes also showed a low performance as sensitizers. According to the results described in Sections 3.1 and 3.2, E5 might have the highest content in CHL, β,β-carotene, echinenone, and zeaxanthin among the evaluated cyanobacterial strains (Bonilla com pers). β,β-carotene and echinenone have similar molecular structures, and their presence decreased the performance of the DSSC for identical reasons. However, due to its strong

fluorescence behavior, CHL does not lead to good efficacy since fluorescence affects the electron transference from the oxidized dye to the semiconductor [72–74]. In contrast, zeaxanthin exhibits the most favorable characteristics for achieving an acceptable PCE because of the -OH presence. The photoanode, predominantly covered by low-performance compounds, leaves a limited area for zeaxanthin or other OH-containing molecules to reach.

Cells sensitized with the extract of strain D3267 were among the most efficient measured at this work. The presence of myxol derivatives, CHL, beta carotene, and echinenone in the absorbance spectrum is assessed for this dye. However, the content of β,β-carotene and echinenone was probably very low because they were not detected using electrochemical techniques. Thus, even though the content of -OH-rich compounds, such as the myxol derivatives, was lower than in the case of MVCC19, the photoanode surface is almost exclusively available for these xanthophylls. Myxoxanthophyll-like derivates and aphanizophyll fulfil the main characteristic requirements for a good sensitizer described above.

What happened to the extracts from the MVCC19 strains? The content of myxoxanthophyll-like derivates and aphanizophyll was very high, with a low amount of CHL, β,β-carotene, and echinenone. In the presence of the MVCC19 pigment, photoanode is mainly covered by the compounds which are more suitable for use as sensitizers. Then, the highest PCE were reached in the presence of this dye. These glycoside-containing compounds are the best among the strains under evaluation, although there are still long-chain structures; therefore, naked spots on the TiO$_2$ surface probably remained. The efficiency is similar to that reported for similar compounds but lower than that reported for smaller compounds like anthocyanins [20–22,36–40,74]. The PCE was 4.2% for cells measured using the N3 dye as a sensitizer, which were constructed and characterized under identical conditions to those used for the pigments mentioned in our present work. This value is lower than 10%, which constitutes the best efficiency reported for this synthetic dye [75]. This shows great potential for the pigments analyzed in this work, but there is a long way to go to improve their performance.

Additional information was deduced from the electrochemical impedance spectroscopy measurements (Figure 4 and Table 4). As previously reported, different circuits were employed to fit the measured profiles [76,77].
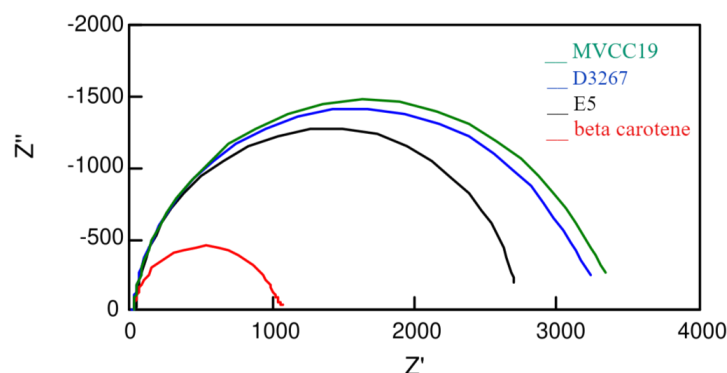
Figure 4. Nyquist plots measured at 0.50 V, in darkness, for the more-efficient cells sensitized with the different dyes analyzed in this work.

An interesting observation concerns the Rce resistance values related to the counter electrode (Table 4). DSSC sensitized with E5 and beta carotene extracts—the less-efficient ones—showed the highest Rce values, supporting the fact that dyes with a high content of compounds without suitable moieties, such as -OH, are able to desorb from the semiconductor surface [19,78]. Once desorbed molecules, such as β,β-carotene and echinenone, diffuse through the liquid electrolyte, they can attach to the counter platinum electrode, increasing the surface's resistance. A platinum surface has better characteristics for the electron transfer occurring at this electrode; therefore, when contaminated by long-chain compounds, the resistance increases.

Table 4. Values obtained from fitting the experimental data measured at V = 0.5 V, in darkness, using a transmission line based model. Γt = the time constant for the transport of the injected electrons that diffuse through the nanoparticle network (calculated as Γt = Rt $\times$ Cμ, with Cμ, the chemical capacitance at the TiO_2/dye/electrolyte interface, associated with the variation in the electron density and the displacement of the Fermi level); Γrec = the recombination time that reflects the lifetime of an electron in the photoanode (calculated as Γrec = Rct $\times$ Cμ); Rce = the resistance associated with the regeneration of I$^-$ at the counter electrode.

	MVCC19	D3267	E5	β,β-Carotene
Γrec = Rct $\times$ Cμ/s	0.018–0.03	0.012–0.02	0.0064	0.0060
Γt = Rt $\times$ Cμ/s	0.0010	0.0016	0.0023	0.0018
Rce/ohm	2	6	22	190

The analysis of the experimental data reveals the crucial importance of high recombination times and time constants. Recombination, for instance, involves the injection of electrons from the semiconductor into the liquid electrolyte. This process, where the electrons generated after the light reaches the pigment's surface followed an undesired path, resulting in decreased PCE. On the other hand, the time constant is about the transport of the injected electrons diffusing through the semiconductor network.

All the analyzed sensitizers showed almost the same time-constant values (Table 4). Then, the performances of the DSSC have to be explained by the differences in the recombination times (Table 4). The ratio between the Γrec and the Γt (and therefore between the Rct and Rt resistances) is useful for understanding the efficiency values. E5 and β,β-carotene dyes have the lowest ratios and also the lowest efficiencies. The differences between them are explained by the Rce values, as explained previously. On the contrary, the most significant ratios are for the dyes of the D3267 and MVCC19 strains. When electrons were generated, they followed transference across the semiconductor instead of recombining with the electrolyte. For the pigments of these two strains, the calculated data values for the recombination time are within a range related to the different applied experimental conditions. As expected, the better DSSC showed the highest Γrec of the range, consistent with what was observed in the case of pigments derived from the D3267 and MVCC19 strains.

EIS data are also helpful in explaining the Voc for the different DSSC evaluated. Voc values rise from the differences between the conduction band edge (and therefore the Fermi level) of the TiO_2 and the redox potential of the electrolyte couple in the assembled devices, according to the following:

$$\Delta V_{OC} = \Delta E_F + \Delta V_{OC} = \Delta E_F + \frac{k_B T}{q} \ln \frac{\Gamma t_1}{\Gamma t_2} \qquad (1)$$

where ΔE_F is the difference between the Fermi levels of the DSSC under comparison; k_B is the Boltzmann constant; q is the electron charge; and Γt are the transport times, as mentioned before.

Remarkably, the experimental conditions during the adsorption process involving the sensitizers affect the conduction band and the Fermi level of the TiO_2.

The difference in the V_{OC} values is confirmed by the observed separation between the Cμ values when exponential dependence between Cμ and the potential begins. Cμ indicates a lower-lying conduction band edge of the TiO_2 for devices containing MVCC19 dyes than those devices containing E5 dyes (Figure 5).

In summary, less-efficient DSSC exhibited a lower V_{OC} of around 0.46 V, while those with the highest PCE boasted a V_{OC} of approximately 0.56 V. The observed tendencies in the capacities and recombination resistances served to reinforce the observed PCE trends.
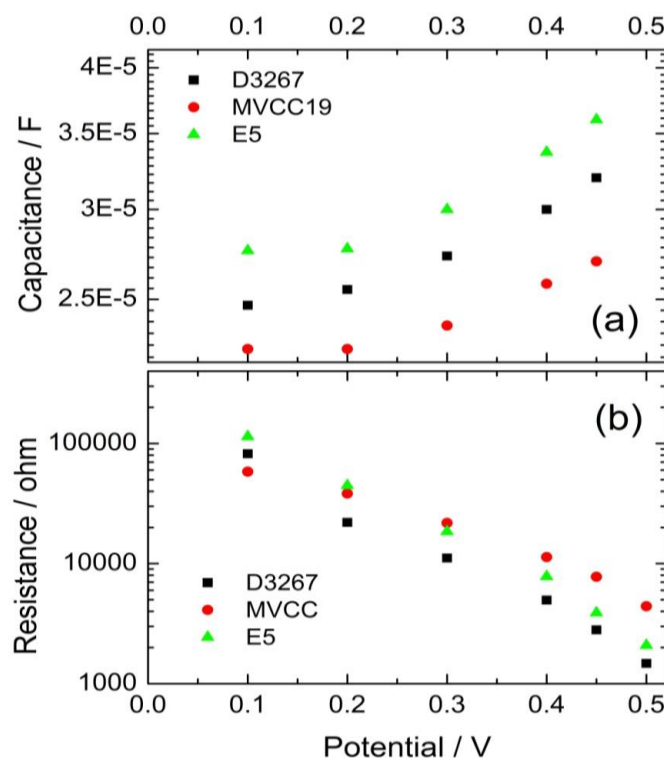
Figure 5. Evolution of the capacitance (**a**) and the recombination resistance (**b**) of the cells, using the pigments extracts of the cyanobacterial strains as sensitizers.

3.4. Thermodynamic Considerations

As mentioned above, dyes need to meet specific criteria to qualify as suitable sensitizers for a DSSC. Electron transfer from its excited state to the conduction band of TiO_2 must be feasible regarding the energy level difference between the dye and the semiconductor. Furthermore, the electrolyte redox couple should regenerate the dye's oxidized form at the counter electrode.

This being said, the Rehm–Weller (RW) equation allows for the estimation of the energy difference between an electron donor (D) and an acceptor (A). In this sense, the Rehm–Weller equation is states the following:

$$\Delta G^0 = e \left[E_D^0 - E_A^0 \right] - E_{0-0} + C \qquad (2)$$

where e corresponds to the number of exchanged electrons; E_D^0 represents the redox potential for the donor oxidized form; E_A^0 corresponds to the acceptor reduced form; E_{0-0} is the energy gap between the excited and the ground-level energy states of the light-absorbing species; and C is the coulombic electrostatic energy between those species. In all cases, the exchanged electrons involved are assumed to be one; the coulombic term is neglected due to the high water dielectric constant and low elementary charge in comparison with the remaining terms.

Considering all of the above, the RW equation simplifies to

$$\Delta G^0 = \left(E_D^0 - E_A^0 \right) - E_{0-0} \qquad (3)$$

For calculations, a value of -0.53 V for the conduction potential of the TiO_2 (named E_A^0 in Equation (3)) is assumed. Moreover, E_D^0 denotes the measured oxidation potential displayed in Section 3.2. Even when the adsorbed dyes affect the conduction potential, as discussed in Section 3.3, the -0.53 V is a reasonable simplification of the calculation performed here [19].

From the normalized excitation and fluorescence emission spectra, it is possible to determine the intersection point (Figure 6). From this intersection, the E_{0-0} values can be calculated using Planck's equation. For example, for MVCC19, and as deduced from Figure 6, the intersection can be determined at 536 nm. Then, using Planck's equation and the RW equation, an E_{0-0} = 2.4 eV and ΔG^0 = −0.39 eV can be calculated (Table 5). The process is favorable, and electron transfer between the dye and the semiconductor occurs. Table 5 summarizes the calculated data for all the evaluated dyes. According to the thermodynamics considerations followed by the RW approach, it is possible to conclude that all the dyes evaluated can transfer their electrons to the semiconductor after absorbing the incident sunlight.
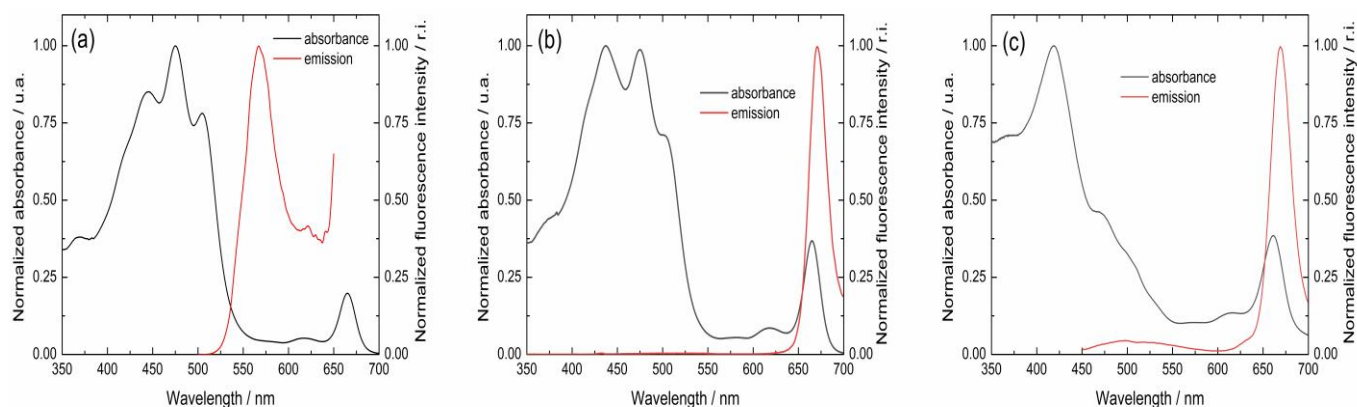
Figure 6. Normalized visible absorption and emission spectra for the pigments named (**a**) MVCC19, (**b**) D3267, and (**c**) E5.

Table 5. Intersection point (in nm) between the normalized excitation and the fluorescence emission spectra for the evaluated dyes; energy gap (E_{0-0}) between the excited and the ground levels for the energy states of the dyes; and free energy difference calculated using the Rehm–Weller equation for the applied sensitizers.

Dye	Wavelength/nm	E_{0-0}/eV	ΔG^0/eV
MVCC19	536	2.40	−0.39
D3267	517	2.31	−0.72
E5	614	2.02	−0.22
β,β-carotene	432	2.87	−0.54

4. Conclusions

In this work, pigments produced by cyanobacterial strains were analyzed as sensitizers for DSSC. Even considering the fact that they produce a mixture of compounds, with their composition depending on the growth conditions (i.e., the light intensity and time), some facts can be highlighted. In a DSSC, the characteristics of the applied sensitizers or mixture of compounds are crucial to assure acceptable power conversion efficiency. Electron transference between the dye and the titanium dioxide is the first relevant step. Then, the semiconductor surface must be completely covered without naked spots remaining, and the presence of -OH moieties is of great importance in allowing bond formation between the dye and the TiO_2 (and also in avoiding the desorption of the attached molecule). Also, the dyes' oxidation potential must ensure dye regeneration. Moreover, pigments must have very low fluorescence emission.

The MVCC19 strains produced a mixture of lipidic pigments with a high content of myxo xanthophyll-like derivates and aphanizophyll, compounds fulfilling most of the essential characteristics of an efficient sensitizer and showing the highest PCE in the tested

DSSC. The opposite was found for the extracts of the E5 strain, which had high CHL, β,β-carotene, and echinenone contents. These compounds epitomize what cannot happen in a sensitizer: the absence of moieties able to coordinate with the titanium, which are therefore capable of desorption, present also fluorescence decay and have a low oxidation potential.

The DSSC efficiency found in this study is higher than that previously reported for DSSC with similar sensitizers extracted from natural sources, indicating the need for further studies investigating cyanobacterial species rich in myxoxanthopylls as potential molecules of great relevance to the sensitivity of solar cells.

References

1. O'Regan, B.; Grätzel, M. A low-cost, high-efficiency solar cell based on dye-sensitized colloidal TiO$_2$ films. *Nature* **1991**, *353*, 737–740. [CrossRef]
2. Zou, J.; Wang, Y.; Baryshnikov, G.; Luo, J.; Wang, X.; Ågren, H.; Li, C.; Xie, Y. Efficient Dye-Sensitized Solar Cells Based on a New Class of Doubly Concerted Companion Dyes. *ACS Appl. Mater. Interfaces* **2022**, *14*, 33274–33284. [CrossRef] [PubMed]
3. Bisquert, J.; Cahen, D.; Hodes, G.; Rühle, S.; Zaban, A. Physical Chemical Principles of Photovoltaic Conversion with Nanoparticulate, Mesoporous Dye-Sensitized Solar Cells. *J. Phys. Chem. B* **2004**, *108*, 8106–8118. [CrossRef]
4. Zhang, D.; Stojanovic, M.; Ren, Y.; Cao, Y.; Eickemeyer, F.T.; Socie, E.; Vlachopoulos, N.; Moser, J.-E.; Zakeeruddin, S.M.; Hagfeldt, A.; et al. A molecular photosensitizer achieves a Voc of 1.24 V enabling highly efficient and stable dye-sensitized solar cells with copper(II/I)-based electrolyte. *Nat. Commun.* **2021**, *12*, 1777. [CrossRef] [PubMed]
5. Khan, M.; Iqbal, M.A.; Malik, M.; Hashmi, S.U.; Bakhsh, S.; Sohail, M.; Qamar, M.T.; Al-Bahrani, M.; Capangpangan, R.Y.; Alguno, A.C.; et al. Improving the efficiency of dye-sensitized solar cells based on rare-earth metal modified bismuth ferrites. *Sci. Rep.* **2023**, *13*, 3123. [CrossRef]
6. Boschloo, G. Improving the Performance of Dye-Sensitized Solar Cells. *Front. Chem.* **2019**, *7*, 77. [CrossRef]
7. Sil, M.C.; Chen, L.S.; Lai, C.W.; Lee, Y.H.; Chang, C.C.; Chen, C.M. Enhancement of power conversion efficiency of dye-sensitized solar cells for indoor applications by using a highly responsive organic dye and tailoring the thickness of photoactive layer. *J. Power Sources* **2020**, *479*, 229095. [CrossRef]
8. Ren, Y.; Zhang, D.; Suo, J.; Cao, Y.; Eickemeyer, F.T.; Vlachopoulos, N.; Zakeeruddin, S.M.; Hagfeldt, A.; Grätzel, M. Hydroxamic acid preadsorption raises efficiency of cosensitized solar cells. *Nature* **2023**, *613*, 60–65. [CrossRef]
9. Solar–IEA–International Energy Agency. Available online: https://www.iea.org/energy-system/renewables/solar-pv (accessed on 21 June 2024).
10. Pouras, H.H.; Barenji, R.V.; Khojastehnezhad, V.M. Solar energy status in the world: A comprehensive review. *Energy Rep.* **2023**, *10*, 3474–3493. [CrossRef]
11. International Renewable Energy Agency IRENA. Renewable Power: Sharply Falling Generation Costs. Available online: https://www.irena.org/-/media/Files/IRENA/Agency/Publication/2017/Nov/%20IRENA_Sharply_falling_costs_2017.pdf (accessed on 21 June 2024).
12. Victoria, M.; Haegel, N.; Peters, I.M.; Sinton, R.; Jäger-Waldau, A.; del Cañizo, C.; Breyer, C.; Stocks, M.; Blakers, A.; Kaizuka, I.; et al. Solar photovoltaics is ready to power a sustainable future. *Joule* **2021**, *5*, 1041–1056. [CrossRef]
13. Cannavale, A.; Martellotta, F.; Fiorito, F.; Ayr, U. The Challenge for Building Integration of Highly Transparent Photovoltaics and Photoelectrochromic Devices. *Energies* **2020**, *13*, 1929. [CrossRef]

14. Muñoz-Garcia, A.B.; Benesperi, I.; Boschloo, G.; Concepcion, J.J.; Delcamp, J.H.; Gibson, E.A.; Meyer, G.J.; Pavone, M.; Pettersson, H.; Hagfeldt, A.; et al. Dye-sensitized solar cells strike back. *Chem. Soc. Rev.* **2021**, *50*, 12450–12550. [CrossRef] [PubMed]

15. Roy, A.; Ghosh, A.; Bhandari, S.; Selvaraj, P.; Sundaram, S.; Mallick, T.K. Color Comfort Evaluation of Dye-Sensitized Solar Cell (DSSC) Based Building-Integrated Photovoltaic (BIPV) Glazing after 2 Years of Ambient Exposure. *J. Phys. Chem. C* **2019**, *123*, 23834–23837. [CrossRef]

16. Lu, L.; Ya'acob, M.E.; Anuar, M.S.; Chen, G.; Othman, M.H.; Noor Iskandar, A.; Roslan, N. Thermal analysis of a portable DSSC mini greenhouse for botanical drugs cultivation. *Energy Rep.* **2020**, *6*, 238–253. [CrossRef]

17. Mariotti, N.; Bonomo, M.; Fagiolari, L.; Barbero, N.; Gerbaldi, C.; Bella, F.; Barolo, C. Recent advances in eco-friendly and cost-effective materials towards sustainable dye-sensitized solar cells. *Green Chem.* **2020**, *22*, 7168–7218. [CrossRef]

18. Ursu, D.; Vajda, M.; Miclau, M. Highly efficient dye-sensitized solar cells for wavelength-selective greenhouse: A promising agrivoltaic system. *Int. J. Energy Res.* **2022**, *46*, 18550–18561. [CrossRef]

19. Cerdá, M.F. Dyes from the Southern Lands: An Alternative or a Dream? *Solar* **2022**, *2*, 519–539. [CrossRef]

20. Montagni, T.; Rodríguez Chialanza, M.; Cerdá, M.F. Blueberries as a Source of Energy: Physical Chemistry Characterization of Their Anthocyanins as Dye-Sensitized Solar Cells' Sensitizers. *Solar* **2023**, *3*, 283–297. [CrossRef]

21. Calogero, G.; Bartolotta, A.; Di Marco, G.; Di Carlo, A.; Bonaccorso, F. Vegetable-based dye-sensitized solar cells. *Chem. Soc. Rev.* **2015**, *44*, 3244–3495. [CrossRef]

22. Calogero, G.; Yum, J.H.; Sinopoli, A.; Di Marco, G.; Grätzel, M.; Nazeeruddin, M.K. Anthocyanins and betalains as light-harvesting pigments for dye-sensitized solar cells. *Sol. Energy* **2012**, *86*, 1563–1575. [CrossRef]

23. Ndiaye, A.; Dioum, A.; Oprea, C.I.; Dumbrava, A.; Lungu, J.; Georgescu, A.; Moscalu, F.; Gîr¸tu, M.A.; Beye, A.C.; Youm, I. A Combined Experimental and Computational Study of Chrysanthemin as a Pigment for Dye-Sensitized Solar Cells. *Molecules* **2021**, *26*, 225. [CrossRef] [PubMed]

24. Aslan, F. New natural dyes extracted by ultrasonic and soxhlet method: Effect on dye-sensitized solar cell photovoltaic performance. *Opt. Quant. Electron.* **2024**, *56*, 645. [CrossRef]

25. Narayan, M.R. Review: Dye sensitized solar cells based on natural photosensitizers. *Renew. Sustain. Energy Rev.* **2012**, *16*, 208–215. [CrossRef]

26. Zhou, H.; Wu, L.; Gao, Y.; Ma, T. Dye-sensitized solar cells using 20 natural dyes as sensitizers. *J. Photochem. Photobiol. A Chem.* **2011**, *219*, 188–194. [CrossRef]

27. Al-Alwani, M.A.M; Mohamad, A.B.; Ludin, N.A.; Kadhum, A.A.H.; Sopian, K. Dye-sensitised solar cells: Development, structure, operation principles, electron kinetics, characterisation, synthesis materials and natural photosensitisers. *Renew. Sustain. Energy Rev.* **2016**, *65*, 183–213. [CrossRef]

28. Richhariya, G.; Kumar, A.; Tekasakul, P.; Gupta, B. Natural dyes for dye sensitized solar cell: A review. *Renew. Sustain. Energy Rev.* **2017**, *69*, 705–718. [CrossRef]

29. Shukor, N.I.A.; Chan, K.Y.; Thien, G.S.H.; Yeoh, M.E.; Low, P.L.; Devaraj, N.K.; Ng, Z.N.; Yap, B.K. A Green Approach to Natural Dyes in Dye-Sensitized Solar Cells. *Sensors* **2023**, *23*, 8412. [CrossRef]

30. da Conceição, L.R.B.; da Cunha, H.O.; Leite, A.M.B.; Suresh Babu, R.; Raja, S.; Ribeiro, C.; de Barros, A.L.F. Evaluation of Solar Conversion Efficiency in Dye-sensitized Solar Cells Using Natural Dyes Extracted from Alpinia purpurata and Alstroemeria Flower Petals as Novel Photosensitizers. *Colorants* **2023**, *2*, 618–631. [CrossRef]

31. Ren, Y.; Flores-Díaz, N.; Zhang, D.; Cao, Y.; Decoppet, J.D.; Fish, G.C.; Moser, E.; Zakeeruddin, S.M.; Wang, P.; Hagfeldt, A.; et al. Blue Photosensitizer with Copper(II/I) Redox Mediator for Efficient and Stable Dye-Sensitized Solar Cells. *Adv. Funct. Mater.* **2020**, *30*, 2004804. [CrossRef]

32. Cai, L.; Moehl, T.; Moon, S.J.; Decoppet, J.D.; Humphry-Baker, R.; Xue, Z.; Bin, L.; Zakeeruddin, S.M.; Grätzel, M. 4,9-Dihydro-4,4,9,9-tetrahexyl-s-indaceno[1,2-b:5,6-b′]dithiophene as a π-Spacer of Donor–π–Acceptor Dye and Its Photovoltaic Performance with Liquid and Solid-State Dye-Sensitized Solar Cells. *Org. Lett.* **2014**, *16*, 106–109. [CrossRef]

33. Kay, A.; Grätzel, M. Low cost photovoltaic modules based on dye sensitized nanocrystalline titanium dioxide and carbon powder. *Sol. Energy Mater. Sol. Cells* **1996**, *44*, 99–117. [CrossRef]

34. Fabregat-Santiago, F.; Bisquert, J.; Garcia-Belmonte, G.; Boschloo, G.; Hagfeldt, A. Influence of electrolyte in transport and recombination in dye-sensitized solar cells studied by impedance spectroscopy. *Sol. Energy Mater. Sol. Cells* **2005**, *87*, 117–131. [CrossRef]

35. Hardin, B.; Snaith, H.; McGehee, M. The renaissance of dye-sensitized solar cells. *Nat. Photon* **2012**, *6*, 162–169. [CrossRef]

36. Orona-Navar, A.; Aguilar-Hernández, I.; Nigam, K.D.P.; Cerdán-Pasarán, A.; Ornelas-Soto, A. Alternative sources of natural pigments for dye-sensitized solar cells: Algae, cyanobacteria, bacteria, archaea and fungi. *J. Biotechnol.* **2021**, *332*, 29–53. [CrossRef] [PubMed]

37. Singh, A.; Mukherjee, T. Application of carotenoids in sustainable energy and green electronics. *Mater. Adv.* **2022**, *3*, 1341–1358. [CrossRef]

38. Alhorani, S.; Kumar, S.; Genwa, M.; Meena, P.L. Performance of dye-sensitized solar cells extracted dye from wood apple leaves. *J. Phys. Commun.* **2022**, *6*, 085012. [CrossRef]

39. Adedokun, O.; Adedeji, O.L.; Bello, I.T.; Awodele, M.K.; Awodugba, A.O. Fruit peels pigment extracts as a photosensitizer in ZnO-based Dye-Sensitized Solar Cells. *Chem. Phys. Impact* **2021**, *3*, 100039. [CrossRef]

40. Orona-Navar, A.; Aguilar-Hernández, I.; Cerdán-Pasarán, A.; López-Luke, T.; Rodríguez-Delgado, M.; Cárdenas-Chávez, D.L.; Cepeda-Pérez, E.; Ornelas-Soto, N. Astaxanthin from Haematococcus pluvialis as a natural photosensitizer for dye-sensitized solar cell. *Algal Res.* **2017**, *26*, 15–24. [CrossRef]

41. Rowan, K.S. *Photosynthetic Pigments of Algae*; Cambridge University Press: Cambridge, UK, 1989.

42. Takaichi, S.; Mochimaru, M. Carotenoids and carotenogenesis in cyanobacteria: Unique ketocarotenoids and carotenoid glycosides. *Cell. Mol. Life Sci.* **2007**, *64*, 2607–2619. [CrossRef]

43. Whitton, B.A. *Ecology of Cyanobacteria II: Their Diversity in Space and Time*; Springer: Dordrecht, The Netherlands, 2012.

44. Bonilla, S.; Cremella, B.; Acuña, V.; Haakonsson, S. Pigment assemblages in subtropical bloom-forming cyanobacteria strains. *J. Plankton Res.* **2023**, *45*, 746–750. [CrossRef]

45. Vézina, S.; Vincent, W. Arctic cyanobacteria and limnological properties of their environment: Bylot Island, Northwest Territories, Canada (73 N, 80 W). *Polar Biol.* **1997**, *17*, 523–534. [CrossRef]

46. Żbik, P.; Kłodawska, K.; Malec, P. The effect of solvent on the optical properties of myxoxanthophyll from Synechocystis sp. PCC6803. *J. Mol. Liq.* **2023**, *375*, 121367. [CrossRef]

47. Bonilla, S. Sección Limnología, Instituto de Instituto de Ecología y Ciencias Ambientales, Facultad de Ciencias, UdelaR., Montevideo, Uruguay. Unpublished work. 2024.

48. Allen, M.M.; Stanier, R.Y. Selective isolation of blue-green algae from water and soil. *J. Gen. Microbiol* **1968**, *51*, 203–209. [CrossRef] [PubMed]

49. Sharmila, S.; Das, M.P.; Seshiah, C.; Rebecca, L.J. Extraction and purification of carotenoids from vegetables. *J. Chem. Pharm. Res.* **2014**, *6*, 594–598.

50. de Bon, M.; Rodríguez Chialanza, M.; Cerdá, M.F. Fucoxanthin from the Antarctic Himantothallus grandifollius as a sensitizer in DSSC. *J. Iran. Chem. Soc.* **2022**, *19*, 3627–3636. [CrossRef]

51. Polyakov, N.E.; Focsan, A.L.; Bowman, M.K.; Kispert, L.D. Free Radical Formation in Novel Carotenoid Metal Ion Complexes of Astaxanthin. *J. Phys. Chem. B* **2010**, *114*, 16968–16977. [CrossRef]

52. Ashenafi, E.L.; Nyman, M.C.; Shelley, J.T.; Mattson, N.S. Spectral properties and stability of selected carotenoid and chlorophyll compounds in different solvent systems. *Food Chem. Adv.* **2023**, *2*, 100178. [CrossRef]

53. Hertzberg, S.; Liaaen-Jensen, S. The constitution of aphanizophyll. *Phytochem.* **1971**, *10*, 3251–3252. [CrossRef]

54. Takaichi, S.; Mochimaru, M.; Maoka, T.; Katoh, H. Myxol and 4-Ketomyxol 2′-Fucosides, not Rhamnosides, from Anabaena sp. PCC 7120 and Nostoc punctiforme PCC 73102, and Proposal for the Biosynthetic Pathway of Carotenoids. *Plant Cell Physiol.* **2005**, *46*, 497–504. [CrossRef]

55. Takaichi, S.; Maoka, T.; Mochimaru, M. Unique Carotenoids in the Terrestrial Cyanobacterium Nostoc commune NIES-24: 2-Hydroxymyxol 20-Fucoside, Nostoxanthin and Canthaxanthin. *Curr. Microbiol.* **2009**, *59*, 413–419. [CrossRef]

56. Foppen, F.H. Tables for the identification of carotenoid pigments. *Chromatogr. Rev.* **1971**, *14*, 133–298. [CrossRef] [PubMed]

57. Hertzberg, S.; Jensen, S.L. The carotenoids of blue-green algae II: The carotenoids of Aphanizomenon flos-aquae. *Phytochemistry* **1966**, *5*, 565–570. [CrossRef]

58. Hertzberg, S.; Jensen, S.L. The structure of myxoxanthophyll. *Phytochemistry* **1969**, *8*, 1259–1280. [CrossRef]

59. Srivastava, A.; Thapa, S.; Chakdar, H.; Babele, P.K.; Shukla, P. Cyanobacterial myxoxanthophylls: Biotechnological interventions and biological implications. *Crit. Rev. Biotechnol.* **2022**, *44*, 63–77. [CrossRef]

60. Mohamed, H.E.; van de Meene, A.M.L.; Roberson, R.W.; Vermaas, W.F.J. Myxoxanthophyll Is Required for Normal Cell Wall Structure and Thylakoid Organization in the Cyanobacterium Synechocystis sp. Strain PCC 6803. *J. Bacteriol.* **2005**, *187*, 6883–6892. [CrossRef]

61. Liu, D.; Gao, Y.; Kispert, L.D. Electrochemical properties of natural carotenoids. *J. Electroanal. Chem.* **2000**, *488*, 140–150. [CrossRef]

62. Hapiot, P.; Kispert, L.D.; Konovalov, V.V.; Saveant, J.M. Single Two-Electron Transfers vs Successive One-Electron Transfers in Polyconjugated Systems Illustrated by the Electrochemical Oxidation and Reduction of Carotenoids. *J. Am. Chem. Soc.* **2001**, *123*, 6669–6677. [CrossRef]

63. Cizmek, L.; Komorsky-Lovric, S. Study of Electrochemical Behaviour of Carotenoids in Aqueous Media. *Electroanalysis* **2019**, *31*, 83–90. [CrossRef]

64. Ishikita, H.; Loll, B.; Biesiadka, J.; Saenger, W.; Knapp, E.W. Redox potentials of chlorophylls in the photosystem II reaction center. *Biochem* **2005**, *44*, 4118–4124. [CrossRef]

65. Enciso, P.; Cerdá, M.F. Solar cells based on the use of photosensitizers obtained from Antarctic red algae. *Cold Regions Sci. Technol.* **2016**, *126*, 51–54. [CrossRef]

66. Edge, R.; Land, E.J.; McGarvey, D.; Mulroy, L.; Truscott, G. Relative One-Electron Reduction Potentials of Carotenoid Radical Cations and the Interactions of Carotenoids with the Vitamin E Radical Cation. *J. Am. Chem. Soc.* **1998**, *120*, 4087–4090. [CrossRef]

67. Shono, T.; Matsumura, Y.; Nakagawa, Y. Electroorganic chemistry. XII. Anodic oxidation of enol esters. *J. Am. Chem. Soc* **1974**, *96*, 3532–3536. [CrossRef]

68. Kleinová, M.; Hewitt, M.; Brezová, V.; Madden, J.C.; Cronin, M.T.D.; Valko, M. Antioxidant properties of carotenoids: QSAR prediction of their redox potentials. *Gen. Physiol. Biophys.* **2007**, *26*, 97–103.

69. Boschloo, G.; Hagfeldt, A. Characteristics of the Iodide/Triiodide Redox Mediator in Dye-Sensitized Solar Cells. *Acc. Chem. Res.* **2009**, *42*, 1819–1826. [CrossRef]

70. Barea, E.M.; Bisquert, J. Properties of chromophores determining recombination at TiO$_2$-dye-electrolyte interface. *Langmuir* **2013**, *29*, 8773–8781. [CrossRef]

71. Hou, R.; Yuan, S.; Ren, X.; Zhao, Y.; Wang, Z.; Zhang, M.; Li, D.; Shi, L. Effects of acetyl acetone-typed co-adsorbents on the interface charge recombination in dye-sensitized solar cell photoanodes. *Electrochim. Acta* **2015**, *154*, 190–196. [CrossRef]

72. Kalaji, H.M.; Schansker, G.; Brestic, M.; Bussotti, F.; Calatayud, A.; Ferroni, L.; Goltsev, V.; Guidi, L.; Jajoo, A.; Li, P.; et al. Frequently asked questions about chlorophyll fluorescence, the sequel. *Photosynth Res.* **2017**, *132*, 13–66. [CrossRef]

73. Yañuk, J.G.; Cabrerizo, F.M.; Dellatorre, F.G.; Cerdá, M.F. Photosensitizing role of R-phycoerythrin red protein and β-carboline alkaloids in Dye sensitized solar cell. Electrochemical and spectroscopic characterization. *Energy Rep.* **2020**, *6*, 25–36. [CrossRef]

74. Enciso, P.; Decoppet, J.D.; Grätzel, M.; Wörner, M.; Cabrerizo, F.M.; Cerdá, M.F. A cockspur for the DSS cells: Erythrina crista-galli sensitizers. *Spectrochim. Acta A Mol. Biomol. Spectrosc.* **2017**, *176*, 91–98. [CrossRef]

75. Nazeeruddin, M.K.; Kay, A.; Rodicio, I.; Humphry-Baker, R.; Mueller, E.; Liska, P.; Vlachopoulos, N.; Graetzel, M. Conversion of light to electricity by cis-X2bis (2,2′-bipyridyl-4,4′-dicarboxylate) ruthenium(II) charge-transfer sensitizers (X = Cl-, Br-, I-, CN-, and SCN-) on nanocrystalline titanium dioxide electrodes. *J. Am. Chem. Soc.* **1993**, *115*, 6382–6390. [CrossRef]

76. Bisquert, J. Theory of the impedance of electron diffusion and recombination in a thin layer. *J. Phys. Chem. B* **2002**, *106*, 325–333. [CrossRef]

77. Hagfeldt, A.; Boschloo, G.; Sun, L.; Kloo, L.; Pettersson, H. Dye-sensitized solar cells. *Chem. Rev.* **2010**, *110*, 6595–6663. [CrossRef] [PubMed]

78. Heo, N.; Jun, Y.; Park, J. Dye molecules in electrolytes: New approach for suppression of dye-desorption in dye-sensitized solar cells. *Sci. Rep.* **2013**, *3*, 1712–1718. [CrossRef]